RSC Advances




ROYAL SOCIETY OF CHEMISTRY

www.rsc.org/advances

RSC Advances

ARTICLE

# A novel sensitive and selective electrochemical sensor based on molecularly imprinted polymer at nanoporous gold leaf modified electrode for warfarin sodium determination†

Received 00th January 20xx,Accepted 00th January 20xx

DOI: 10.1039/x0xx00000x

www.rsc.org/

Yingchun Li [a,b]*, Lu Zhang [a], Jiang Liu [a], Shu-Feng Zhou [d], Khalid Abdullah Al-Ghanim [e], Shahid Mahboob [e], Bang-Ce Ye [b], Xueji Zhang [c]*

Warfarin sodium (WFS) is a widely used oral anticoagulant drug but with narrow therapeutic window. Since traditional detection methods applied for therapeutic drug monitoring suffer some shortcomings including difficulty in timely report, high cost and tedious operation, it is necessary to develop a detection system for rapid monitoring of WFS in biological samples. Here we report a novel electrochemical sensor, which was facilely fabricated by coupling nanoporous gold leaf (NPGL) with molecularly imprinted polymer (MIP) to afford ultrasensitive and selective determination of WFS. The morphology characterization via scanning electron microscopy proved successful modification of sensor by NPGL followed with MIP layer modification. Influencing parameters including type of monomer, pH and molar ratio of template to monomer were optimized during electro-polymerization. By using $Fe(CN)_6^{3-/4-}$ as probe as electrical indicator, a linear relationship of current response versus concentration of WFS was obtained in the range from $1.0\times10^{-10}$ to $8.0\times10^{-8}$ M under the optimal experimental conditions, with a detection limit of $4.1\times10^{-11}$ M (S/N=3). In addition, the as-prepared sensor exhibited specific detection of WFS over its structural analogues and interferents, and the established electrochemical approach was validated by the standard method-high performance liquid chromatography. Eventually, rapid and accurate determination of WFS in human blood was carried out after easy sample pretreatment.

## 1. Introduction

Warfarin sodium (WFS), a member of coumarin derivatives, is an oral anticoagulant widely used in multifarious cerebrovascular and cardiovascular disorders, for instance, venous pulmonary embolism, atrial fibrillation, coronary heart diseases, etc. Despite its effectiveness, treatment with warfarin has several shortcomings, one of which is narrow therapeutic window. Dosage out of the window may cause either treatment failure or unwanted bleedings and even threat to life. Therefore, the activity of WFS has to be monitored by blood testing to ensure an adequate yet safe dose[1-4].

The methods of determining WFS in biological samples include high performance liquid chromatography (HPLC) equipped with fluorescence[5] or ultraviolet detectors[6], liquid chromatography–tandem mass spectrometry (LC–MS/MS)[7], capillary zone electrophoresis (CZE)[8], and so on. However, particular concerns for these large instrument-based strategies are high energy and money consumption, long working time, tedious pretreatment, etc., which is especially unsuitable for fast therapeutic drug monitoring. An alternative to the aforementioned techniques is electrochemical sensing, which gains much attention owing to easy preparation, high sensitivity, low detection limit, etc.[9, 10]. Specificity, however, is a common problem for sensor-based determination since normally no separation system is involved in detection procedure. Therefore, physical, chemical or biological modification is often necessary to endow sensor with specific recognition ability toward target molecules[11-14]. A very promising modifier candidate is molecularly imprinted polymer (MIP) since it is able to provide antibody-like specificity and long-term stability[15]. Another barrier encountered in electrochemical sensing is that analytes must have electrochemical activity[16-21], which means redox reaction of the target analyte should happen at sensor surface under certain experimental conditions. As redox reaction conditions for different analytes could have big difference, tedious optimization work is often needed in order to find suitable conditions and achieve sensitive electrical signals. In our previous work, we have developed a versatile way of measuring various substances by introducing active probe as electrical signal indicators (e.g. ferri/ferro-cyanide) along with MIP-modified electrochemical sensor[22-24]. Such strategy is independent on the electrochemical activity of the analyte itself, and thus is possible to test any species by electrochemical sensor.

Apart from specificity and feasibility, another important issue in sensor development is sensitivity. As materials with nanostructure are expected to enlarge the effective surface area of a planar sensor surface, various nano-agents have been employed to modify sensor

[a] School of Pharmacy, Shihezi University, Shihezi 832000, China. E-mail: yingchunli@shzu.edu.cn, Tel/Fax: +86-993-2057005.
[b] Key Laboratory for Green Processing of Chemical Engineering of Xinjiang Bingtuan, School of Chemistry and Chemical Engineering, Shihezi University, Shihezi 832003, China.
[c] Research Center for Bioengineering and Sensing Technology, University of Science and Technology Beijing, Beijing 100083, China. E-mail: zhangxueji@ustb.edu.cn, Tel/Fax: +86-10-62333910.
[d] Department of Pharmaceutical Science, College of Pharmacy, University of South Florida, Tampa, FL 33612, USA.
[e] Department of Zoology, College of Science, King Saud University, P.O. Box 2455, Riyadh-11451, Saudi Arabia.
†Electronic supplementary information (ESI) available. See DOI: XXX

for the purpose of improving sensitivity[25-30]. Among them, a very suitable material is nanoporous gold leaf (NPGL). The unique features of NPGL include high conductivity, interconnected three-dimensional (3D) architecture, uniformly distributed nanopores and nanoligments, good biocompatibility, relatively low cost, and possibility for mass production[31-33]. Compared with gold nanoparticles, NPGL is a free-standing mesoporous thin film with rigid 3D framework structure which avoids particles stacking, thus assuring controllability and stability of NPGL modified sensor. In the present work, we fabricated an electrochemical sensor by combining NPGL and MIP and furthermore the composite-film decorated sensor was applied for detection of WFS. Several parameters influencing the sensing performance have been carefully optimized and the resulted sensor has been successfully adopted to analyze WFS in human blood.

## 2. Experimental

### 2.1 Materials and apparatus

Warfarin sodium (WFS), aspirin (ASP), hydrochlorothiazide (HCT), vitamin $K_4$ ($VK_4$) were obtained from J&K Scientific Ltd. (Beijing, China). phenylenediamine, resorcinol and *o*-aminophenol were purchased from Shanghai Aladdin Co. (Shanghai, China). Dopamine was obtained from Adamas Reagent Co. Ltd. Au/Ag alloy leaves (50:50 wt%; 100 nm in thickness) were purchased from Suzhou ColdStones Tech. Co. Ltd. (Suzhou, China). Human blood samples were obtained from the first affiliated hospital of the medical college of Shihezi University) (Shihezi, China). Reagents and materials, such as starch, sucrose, dextrin glucose, $Fe(CN)_6^{3-/4-}$, NaCl, $CaCl_2$, $NH_4Cl$, $H_2SO_4$, $KNO_3$, $HNO_3$, methanol and phosphate buffer solution (PBS, $KH_2PO_4$ and $K_2HPO_4$) were of analytical grade.

Electrochemical measurements were performed on a CHI 760E Electrochemical Workstation (CHI Instruments Co., Shanghai, China) connected to a PC at room temperature. A conventional three-electrode system was employed, consisting of a bare or a modified planar gold electrode (GE, 4 mm in diameter) as the working electrode, a saturated calomel electrode (SCE) as the reference electrode and a platinum wire (0.5 mm in diameter, 34 mm in length) as the counter electrode. All potentials given in this paper were referred to SCE. The surface morphology of NPGL was characterized with a Zeiss Supra55VP scanning electron microscope (SEM) operating at 20 kV. HPLC was performed with a Shimadzu (Japan) system comprising of LC-10A pumps and an SPD-10A UV-detector. LC condition was as follows: chromatographic separation was performed on a WondaSil $C_{18}$ column (150 mm×4.6 mm i.d., 5 μm) which was purchased from Dalian Elite Analytical Instruments Co. (Dalian, China). The mobile phase for WFS was acetonitrile-methanol-water (70:30:1, v/v/v) with a flow rate of 1.0 mL/min and the detection wavelength was 308 nm.

### 2.2 Preparation of sensor

The Ag/Au alloy leaves were pruned into a 7×7 mm sheet and floated onto the surface of 65 wt% nitric acid. The erosion was stopped after 60 min, and then the sample was washed with distilled water thoroughly and the NPGL was obtained. GE was first polished repeatedly to a mirror finish with 0.3 and 0.05 mm $Al_2O_3$ and utterly cleaned with distilled water before use. NPGL was carefully affixed to GE surface and the NPGL-modified GE (NPGL/GE) was dried under infrared lamp for 15 min. The MIP was electro-polymerized on electrode surface by cyclic voltammetry (CV), which was performed between 0 and 1.0 V (vs. SCE) for 15 cycles at a scan rate of 50 mV/s in solution containing functional monomers and WFS. Afterwards, the polymer film-covered NPGL/GE was immersed in 0.1 M NaOH to remove embedded WFS by scanning from −0.5 V to +0.5 V for several cycles until obvious and stable redox peaks could be found in the probe solution of 5 mM $Fe(CN)_6^{3-/4-}$ and 0.1M KCl. The schematic representation for preparation of WFS-MIP/NPGL/GE is illustrated in Fig. 1. For comparison, non-imprinted polymer (NIP)-modified electrode (NIP/NPGL/GE) was prepared by the same method but in the absence of the template-WFS during electro-polymerization[34].

### 2.3 Electrochemical measurement

Electrochemical behavior of different electrodes was studied in probe solution using CV, which was operated in the scanning range of −0.2~+0.6 V at a scan rate of 100 mV/s. A sensor was first incubated in a sample solution containing analyte for 10 min, after which the electrode was washed with water and applied for voltammetric measurement. The peak current shift ($\Delta I$) was calculated from the reduction peak currents of $Fe(CN)_6^{3-/4-}$ obtained before and after binding with WFS. The shift was used to explore the influence of different modifications on sensor performance and to establish calibration curve for sample determination. After each analysis, the sensor was recovered by immersion in 0.1 M NaOH with CV scanning between −0.5~+0.5 V for several cycles to remove WFS at electrode surface. The electrode was reusable after this cleaning procedure. Electrochemical impedance spectroscopy (EIS) experiments were carried out in a solution containing 5 mM $Fe(CN)_6^{3-/4-}$ and 0.1 M KCl within the frequency range from 0.01 Hz to 100 KHz. All the electrochemical experiments were performed at room temperature.

### 2.4 Detection of WFS in biological samples

A certain amount of WFS was added into human blood sample for spiked recovery experiment. The sample was centrifuged at 4000 rpm for 10 min and methanol was added into the supernatant at volumetric ratio of 1:1, followed by further centrifugation at 4000 rpm for 10 min to get rid of protein. The final supernatant was used for WFS detection.

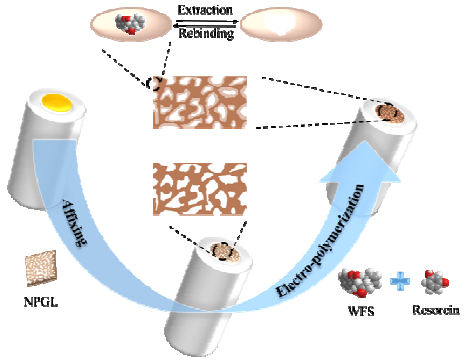


**Fig. 1** Schematic representation of WFS-MIP/NPGL/GE fabrication.

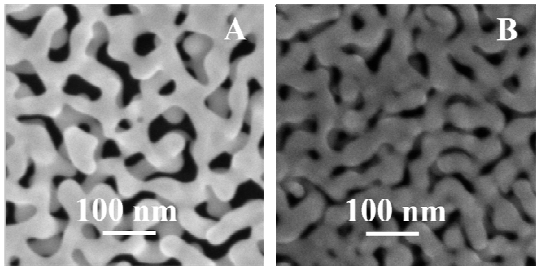


**Fig. 2** SEM images of (A) an NPGL-modified electrode and (B) an MIP-NPGL-modified electrode.

## 3. Results and discussion

### 3.1 Preparation and characterization of WFS-MIP/NPGL/GE electrode

The process of preparing hybrid sensor modified with MIP and NPGL composite film is illustrated in Fig. 1. The morphology of the electrode surface was characterized by SEM, which exhibits a spongy-like conformation with metal ligaments and nanopore channels (Fig. 2A). Modification of NPGL with electro-synthesized MIP layer is obvious as the width of the nanopores decreases from ~30 nm to ~20 nm and the image gets darker compared with bare NPGL (Fig. 2B). Ag/Au alloy leaves, NPGL and molecularly imprinted polymer decorated MIP (MIP/NPGL) after removal of WFS were probed via energy dispersive spectrograph (EDS) and element mapping. All the related information was given in Fig S1, S2, S3 and S4 in Electronic supplementary information file. Compared with EDS spectrum of Ag/Au alloy leaf (Fig. S1a), there are only Au signals in NPGL (Fig. S1b), indicating that Ag was removed after dealloying. When MIP covered the surface of NPGL, elements of carbon and oxygen can be observed from EDS spectra (Fig. S1c), and their relative contents are corresponding to the calculated values of functional monomer (resorcin, $C_6H_6O_2$), which confirms the formation of MIP network on NPGL. From the element mapping images (Fig S2 to S4), one can see that the elements Au, C and O are uniformly distributed on electrode surface, implying that homogeneous MIP film was obtained onto NPGL by in situ electropolymerization of functional monomers. The electrochemical behavior of the stepwise production process was investigated via CV in probe solution. As shown in Fig. 3A, compared with bare GE (curve a), the peak currents of NPGL/GE (curve b) increases obviously due to its enlarged surface area, which can enhance the detection sensitivity. After MIP modification, the redox peaks of $Fe(CN)_6^{3-/4-}$ disappears (curve c). This phenomenon can be explained by that MIP is not conductive and after the whole electrode surface was densely covered with the polymeric film, there was virtually no channel for the active probe ions to access the electrode surface. This also proves successful preparation of WFS-MIP film onto the entire 3D surface of NPGL electrode. After that, removal of template leads to increase of peak currents (curve d), as the cavities generated in the rigid polymer matrix open doors for the probe ions to transfer to the electrolyte/electrode interface. When the electrode was immersed into the solution of WFS, rebinding of WFS by MIP impeded electron transportation of $Fe(CN)_6^{3-/4-}$, resulting in current reduction (curve e).

Electrochemical impedance spectroscopy (EIS) is also a helpful way of characterizing the stepwise sensor construction process and provided useful information on impedance change at the electrode/electrolyte interface[35]. Fig. 3B depicts the EIS diagrams of electrodes at each preparation step. Bare GE (curve a) yielded a small semicircle, implying the electrode has quite good conductivity. In comparison, the semicircle at NPGL/GE (curve b) got much smaller, suggesting that the nanoporous structure of NPGL benefits electron migration effectively. Significant increase in the diameter of the semicircle was observed in curve c, which is ascribed to MIP modification and the polymer acted as a compact barrier for electron transfer. Conductivity of the electrode was recovered by getting rid of template (curve d) due to the cavities created in the polymer matrix. Finally, rebinding of WFS increased the impedance of the electrode (curve e), as a result of WFS embedding in binding sites and consequently inhibiting redox reactions of probe ions.

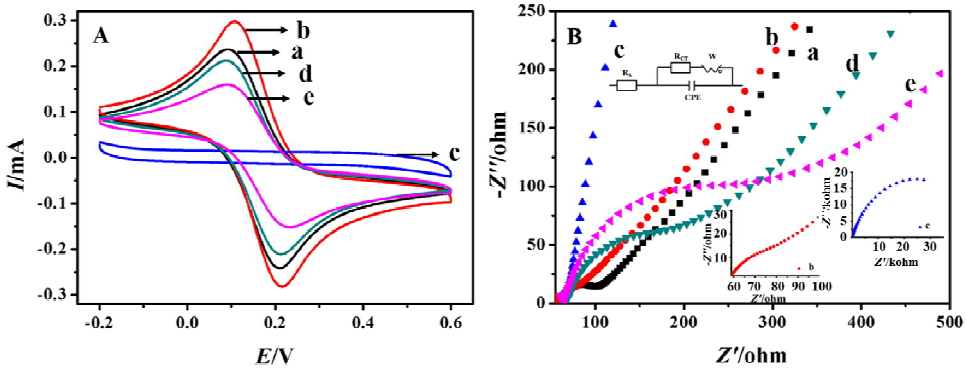


**Fig. 3** Cyclic voltammograms (A) and Nyquist diagrams of EIS (B) for bare GE (a), NPGL/GE (b), MIP/NPGL/GE before extraction of WFS (c), MIP/NPGL/GE after extraction of WFS (d) and MIP/NPGL/GE after rebinding of WFS (e). The insets of (B) are the EIS plots for (b) and (c) in their proper coordinate ranges and the equivalent circuit diagram. The supporting eletrolyte of CV (A) contained 0.1 M $Fe(CN)_6^{3-/4-}$ and 0.1 M $KNO_3$, and that of EIS (B) contained 5 mM $Fe(CN)_6^{3-/4-}$ and 0.1 M KCl. The scan rate of CV (A) was 100 mV $s^{-1}$ and the frequency range of EIS (B) was from 0.01 Hz to 100 kHz

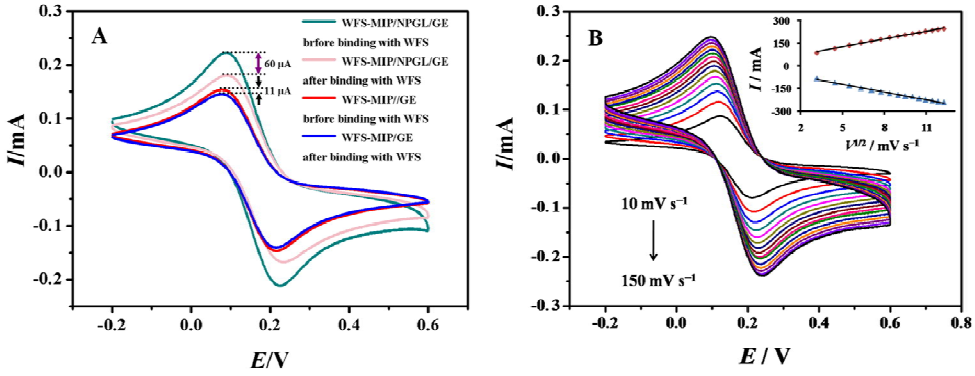


**Fig. 4** Cyclic voltammograms of (A) MIP/NPGL/GE and MIP/GE at a scan rate of 100 mV $s^{-1}$ before and after binding with WFS and of (B) MIP/NPGL/GE at the scan rate from 10 to 150 mV $s^{-1}$. The electrolyte contained 5 mM $Fe(CN)_6^{3-/4-}$ and 0.1 M KCl; the inset of (B) is the anodie and the cathodic peak currents versus square-root of scan rate plot.

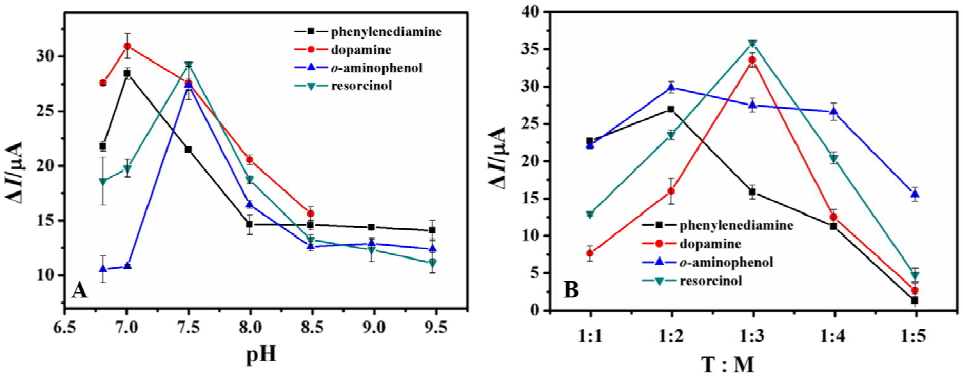


**Fig. 5** Sensing responses toward 1.0 nM WFS by using different MIP/GE prepared with varied monomers and pH values (A) and with varied ratio of template and monomer (T:M) under the individual optimal pH values (B). The T:M was set at 1:3 for (A).All the experiments are repeated in triplet.

In order to investigate the role of NPGL on sensor performance, MIP/GE was prepared as a comparison sensor. Fig. 4A is the cyclic voltammograms of MIP/NPGL/GE and MIP/GE before and after binding with WFS, showing that the current shift of MIP/NPGL/GE is about 5.3 times larger than that of MIP/GE. The enhanced sensing response of the hybrid sensor can be contributed by the nanoporous architecture of NPGL which enhanced the active surface area and the conductivity of the electrode.

Fig. 4B depicts the change in cyclic voltammograms of MIP/NPGL/GE with varying the scan rate. A linear relationship was observed between the redox peak currents and the square root of the scan rate, revealing diffusion-controlled mechanism at the sensor surface [36].

### 3.2 Optimization of MIP/NPGL/GE preparation

*3.2.1 Influence of pH value on electro-polymerization of MIP*

Four monomers (phenylenediamine, dopamine, o-aminophenol and resorcinol) were tested as the functional monomer candidates for achieving the optimal imprinting effect toward WFS. First, pH values during polymerization were optimized for each monomer with the molar ratio of template to monomer (T:M) of 1:3. Since precipitation of WFS occurs when pH value less than 6.8, the pH range in the optimization work started at 6.8. After polymerization and extraction of WFS, the electrodes modified with different MIP films were employed for detection of WFS at the same concentration of $1.0\times10^{-9}$ M and their reduction peak current shifts ($\Delta I$) before and after rebinding of WFS were used to evaluate the individual response level. As shown in Fig. 5A, the optimum pH for, phenylenediamine, dopamine, o-aminophenol and resorcinol are 7.5, 7.0, 7.5 and 7.0, respectively.

*3.2.2 Optimization of the molar ratio of template to monomer (T:M)*

After choosing the most ideal pH value for each monomer, the molar ratio between template molecule and monomer (T:M) was studied in the ratio range from 1:1 to 1:5. The effect of T:M is related to the number of binding sites generated during MIP preparation. Inadequate functional monomer results in insufficient binding sites available for WFS binding, while excessive amount of monomers during polymerization causes thick MIP film on electrode surface, and consequently many binding sites are buried in polymeric matrix and become non-effective. As shown in Fig. 5B, the MIP/GE with resorcinol as the monomer displayed the largest current response to WFS at the pH value of 7.5 and T:M of 1:3.

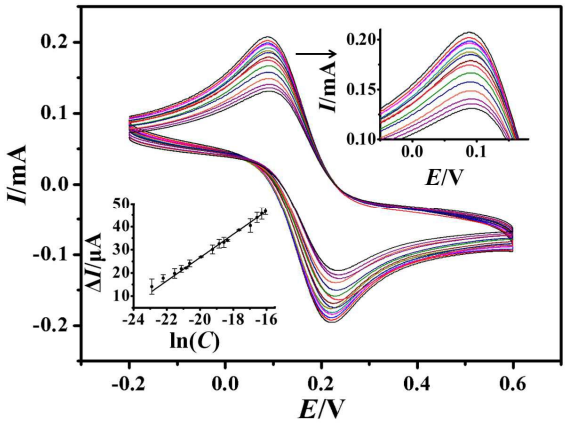


**Fig. 6** Cyclic voltammograms of MIP/NPGL/GE in probe solution after rebinding with WFS in the concentration range of $1\times10^{-10}$~$8\times10^{-8}$ M. The top-right inset shows partially amplified cyclic voltammograms and the bottom-left inset is the calibration curves correlating current shift ($\Delta I$) with the logarithm of concentration of WFS (ln$C$).

### 3.3 Calibration curve and detection limit

Under the optimized experimental conditions, the CV responses and calibration curve for detecting WFS using the proposed MIP/NPGL/GE sensor were investigated. Fig. 6 shows the correlation between the current shift ($\Delta I$) and the logarithm of concentration of WFS (ln$C$), and the corresponding linear regression equations is $\Delta I$ (μA)= 5.2513 ln$C$ + 129.6810 ($R^2$ = 0.9948) in the range of $1\times10^{-10}$~$8\times10^{-8}$ M. The limit of detection (LOD) is down to $4.1\times10^{-11}$ M (S/N=3), which is lower than the data from all the reported WFS sensors we could find. The comparison is summarized in Table 1.

### 3.4 Selectivity of the WFS-MIP/NPGL/GE

In order to assess the specificity of the MIP-modified sensor, HCT, $VK_4$ and ASP, the structural analogues of WFS, were detected. As shown in Fig. 7, the MIP/NPGL/GE exhibited much higher response to WFS than to other analogue, whereas NIP/NPGL/GE shows no obvious difference in sensing all the analytes. The *t*-test shown in Fig. 7A also proved the remarkable difference of sensor response at MIP/NPGL/GE towards analogues and WFS of results with a significant level of 0.01. The high specificity of MIP can be ascribed to the classic molecular imprinting effect[41, 42]. In particular, during MIP preparation, WFS was incorporated into polymeric networks via several kinds of non-covalent interactions and the following removal of WFS left behind the imprinting cavities that are complementary to the template in size, shape and functionality. NIP, due to the lack of imprinting effect, can only yield non-specific binding toward different substances. The calibration curves of WFS and its structural analogues in the range of $1\times10^{-10}$~$8\times10^{-8}$ M are shown in Fig. S5, in order to further investigate the sensitivity of MIP/NPGL/GE towards different compounds. It is obvious that MIP/NPGL/GE has higher current shift for WFS than analogues with the slopes of WFS (0.0531) 3 times larger than that of HCT (0.0139), $VK_4$ (0.0150) and ASP (0.0173). In addition, it is known that some co–existing ions may cause interference on WFS detection in real sample. Hence, the mixture of WFS and several ions ($NH_4^+$, $Ca^{2+}$, $Na^+$, $K^+$, $NO_3^-$, $SO_4^{2-}$ and $Cl^-$) was assayed with the concentration of these ions ten times higher than that of WFS. It was found that the sensing response from WFS alone is 97.8% of the reposne from the mixture, implying excellent anti-interfering ability of MIP/NPGL/GE even in complicated matrix where the amount of interferents is remarkably higher than the analyte.

### 3.5 Repeatability and stability

WFS at three different concentrations ($8\times10^{-8}$, $8\times10^{-9}$ and $8\times10^{-10}$ M) was measured in triplicate using the same MIP/NPGL/GE sensor. Relative standard deviation (RSD) less than 2.5% was obtained, which reflects good repeatability of the sensor. When not in use, all the electrodes were stored in open air at room temperature. Compared with the initial electro-signal, the current response decreased by about 3% over the first week, then little change was

**Table 1** Comparison of the major characteristics of some electrochemical methods for WFS detection.

| Electrodes | Methods | Dynamic range (μM) | LOD (μM) | RSD (%) | References |
|---|---|---|---|---|---|
| AuNP[a]/MIP/f-MWCNT[b]/GCE[c] | square wave voltammetry | $1\times10^{-4}$ ~ $2\times10^{-2}$ | $8\times10^{-5}$ | 2.50 | 37 |
| $Fe_3O_4$/CPE[d] | square wave anodic stripping voltammetry | 0.5 ~ 1000 | 0.21 | 2.30 | 38 |
| CdS-QDs[e]/CS[f]/MWCNTs/GCE | cyclic voltammetry | 0.05 ~ 80 | 8.50 | 2.26 | 39 |
| HMDE[g] | square wave adsorptive cathodic stripping voltammetry | 0.005 ~ 0.4 | $6.5\times10^{-4}$ | - | 40 |
| MIP/NPGL/GE | cyclic voltammetry | $1\times10^{-4}$ ~ $8\times10^{-2}$ | $4.1\times10^{-5}$ | 2.45 | this work |

[a] AuNP: gold nanoparticles, [b] f-MWCNT: multiwall carbon nanotubes containing carboxylic functional group, [c] GCE: glassy carbon electrode, [d] CPE: carbon paste electrode, [e] CdS-QDs: CdS-quantum dots, [f] CS: Chitosan, [g] HMDE: hanging mercury drop electrode
- Not illustrated

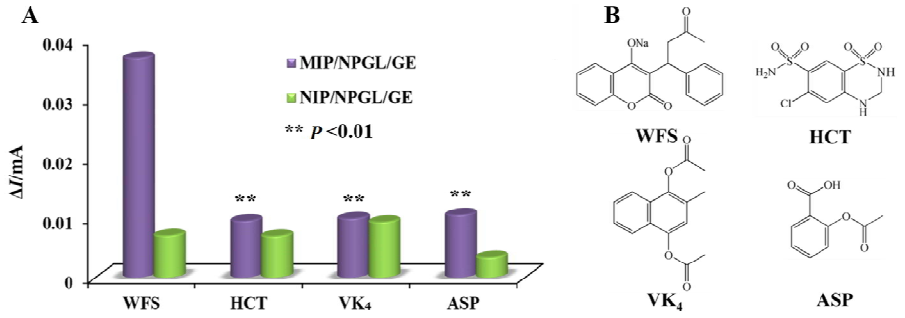


**Fig. 7** Comparison of the sensor responses towards WFS and its structural analogues at the same concentration of $8\times10^{-9}$ M by using MIP/NPGL/GE and NIP/NPGL/GE (A); chemical structures of WFS and its structural analogues (B).

**Table 2** Determination of WFS in human serum using MIP/NPGL/GE and HPLC (n=3)

| Method | Determined | Spiked [a] | Total found [a] | Recovery (%) | RSD (%) |
|---|---|---|---|---|---|
| HPLC | - | 1.600 | 1.575 ± 0.0262 | 98.4 | 1.6 |
| | - | 2.000 | 2.009 ± 0.0066 | 100.0 | 0.3 |
| | - | 2.400 | 2.368 ± 0.0216 | 98.7 | 0.9 |
| WFS-MIP/NPGL/GE | - | 1.600 | 1.659 ± 0.0235 | 103.7 | 1.4 |
| | - | 2.000 | 2.099 ± 0.0595 | 104.9 | 2.8 |
| | - | 2.400 | 2.471 ± 0.1079 | 102.9 | 4.3 |

Mean value ± S.D.
[a] The units of the value is $10^{-5}$ M for HPLC and $10^{-9}$ M for MIP/NPGL/GE.
- Not detected

observed in one-month period of time, exhibiting decent stability of the hybrid electrode, which could be ascribed to the inherent stability of NPGL and MIP.

### 3.6 Real sample analysis

In order to evaluate the capability of the developed sensor in detecting real clinical samples, WFS in human blood was tested. The results shown in Table 2 exhibited satisfying accuracy with recoveries ranging from 102.9 % to 104.9 %. In addition, HPLC was employed as the standard method to analyze the same blood samples and the results were in good accordance with those from our sensor, which proved the validity of the newly developed approach.

## 4. Conclusions

In this study, a novel hybrid sensor system was established by using two-step coating tactic of integrating NPGL modification and in situ MIP electro-synthesis for specific detection of WFS. This is to our knowledge the first report on combination of WFS-imprinted polymeric film with NPGL for establishing hybrid membrane-modified electrochemical sensor. First of all, 3D open and continuous nanoporous skeleton of NPGL helps enhance electron transmission on one hand and allow for enlarged platform for MIP loading on the other. Secondly, MIP layer provides a number of imprinting cavities that match template molecules based on geometrical size and the number and the steric arrangement of functional groups, guaranteeing the specific recognition toward WFS. Application of the modified electrode in real sample analysis is proved to be more sensitive and convenient than the reference method-HPLC with comparable accuracy and repeatability. Compared with the reported work of other systems, the sensor fabrication technique is facile and highly controllable, ensuring very good reproducibility and easiness for developing admirable sensors in mass production. In summary, the sensor preparation procedure is simple and cost-effective, and the detection of WFS is far quicker than the commonly employed method-HPLC. Therefore, it can be expected that the developed sensor has great potential in therapeutic drug monitoring.

## Acknowledgements

The project financially supported by National Natural Science Foundation of China (81260487, 81460543), the Pairing Program of Shihezi University with Eminent Scholar in Elite University (SDJDZ201502). The authors would like to express their sincere appreciation to the Deanship of Scientific Research at King Saud University for its funding of this research through the Research Group Project No. Prolific Research Group No. 1436-011.

## Notes and references

1 D. M. Ufer, *Clin. Pharmacokinet*, 2005, **44**, 1227-1246.
2 R. Hull, G. Raskob, G. Pineo, D. Rosenbloom, W. Evans, T. Mallory, K. Anquist, F. Smith, G. Hughes and D. Green, *New Engl. J. Med.*, 1993, **329**, 1370-1376.
3 R. Hull, T. Delmore, E. Genton, J. Hirsh, M. Gent, D. Sackett, D. Mcloughlin and P. Armstrong, *New Engl. J. Med.,* 1979, **301,** 855-858.
4 L. Wallentin, S. Yusuf, M.D. Ezekowitz, M. Alings, M. Flather, M.G. Franzosi, P. Pais, A. Dans, J. Eikelboom and J. Oldgren, *Lancet*, 2010, **376**, 975-983.
5 C. Banfield and M. Rowland, *J. Pharm. Sci.*, 1984, **73**, 1392-1396.
6 P. R. Ring and J. M. Bostick, *J. Pharmaceut. Biomed.*, 2000, **22**, 573-581.
7 M. J. Kwon, H. J. Kim, J. W. Kim, K. H. Lee, K. H. Sohn, H. J. Cho, Y. K. On, J. S. Kim and S. Y. Lee, *Korean J. Lab. Med.*, 2009, **29**, 515-523.
8 W. P. Yau and E. Chan, *J. Pharmaceut. Biomed.*, 2002, **28**, 107-123.
9 P. Y. Chen, P. C. Nien, C. W. Hu and K. C. Ho, *Sensor. Actuat. B-Chem.*, 2010, **146**, 466-471.
10 M. A. Radwan, G. A. Bawazeer, N. M. Aloudah, B. T. AlQuadeib and H. Y. Aboul-Enein, *Biomed. Chromatogr.*, 2012, **26**, 6-11.
11 X. L. Chai, X. G. Zhou, A. W. Zhu, L. M. Zhang, Y. Qin, G. Y. Shi and Y. Tian, *Angew. Chem. Int. Ed.*, 2013, **52**, 8129-8133.
12 C. Zheng , X. L. Zhang W. Liu, B. Liu, H. H. Yang, Z. A. Lin and G. N. Chen, *Adv. Mater.*, 2013, **25**, 5922-5927.
13 W. J. Lian, S. Liu, J. H. Yu, J. Li, M. Cui, W. Xu and J. D. Huang, *Biosens. Bioelectron.*, 2013, **44**, 70-76.
14 X. B. Zhang, Z. D. Wang, H. Xing, Y. Xiang and Y. Lu, *Anal. Chem.*, 2010, **82**, 5005-5011.
15 M. L. Yola, T. Eren and N. Atar, *Sensor. Actuat. B-Chem*., 2014, **195**, 28-32
16 X. Yi, J. Huang-Xian and C. Hong-Yuan, *Anal. Biochem.*, 2000, **278**, 22-28.
17 M. L. Yola, T. Eren and N. Atar, *Biosens. Bioelectron*., 2014, **60**, 277-285.
18 A. Salimi, M. Izadi, R. Hallaj and M. Rashidi, *Electroanal.*, 2007, **19**, 1668-1676.
19 M. L. Yola, L. Uzun, N. Özaltın and A. Denizli, *talanta*, 2014, **120**, 318- 324.
20 V. C. Sanz, M. L. Mena, A. González-Cortés, P. Yanez-Sedeno and J. Pingarrón, *Anal. Chim. Acta*, 2005, **528**, 1-8.
21 Y. Li, X. Fan, J. Qi, J. Ji, S. Wang, G. Zhang and F. Zhang, *Mater. Res. Bull.*, 2010, **45**, 1413-1418.
22 Y. Liu, J. Liu, H. Tang, J. Liu, B. Xu, F. Yu and Y. C. Li, *Sensor. Actuat. B-Chem.*, 2015, **206**, 647-652.
23 Y. C. Li, Y. Liu, J. Liu, J. Liu, H. Tang, C. Cao, D. Zhao and Y. Ding, *Sci. Rep.*, 2015, **5**, 7699-7706.
24 Y. C. Li, H. Song, L. Zhang, P. Zuo, B. C. Ye, J. Yao and W. Chen, *Biosens. Bioelectron.*, 2016, **78**, 308-314.
25 C. Ho, D. W. M. Sin, K. M. Wong and H. P. O. Tang, *Anal. Chim. Acta*, 2005, **530**, 23-31.
26 X. X. Dong, M. Y. Li, N. N. Feng, Y. M. Sun, C. Yang and Z. L. Xu, *RSC Adv.*, 2015, **5**, 86485-86489.
27 K. Zangeneh Kamali, A. Pandikumar, G. Sivaraman, H. N. Lim, S. P. Wren, T. Sun and N. M. Huang, *RSC Adv.*, 2015, **5**, 17809 17816
28 M. L. Yola, N. Atar and T. Eren, Sensor. Actuat. B-Chem., 2014, 198, 70-76.
29 B. C. Yin, S. Wu, J. L. Ma and B. C. Ye, *Biosens. Bioelectron.*, 2015, **68**, 365-370.
30 V. K. Gupta, M. L. Yola, N. Özaltın, N. Atar and Z. Üstündağ, Electrochim. Acta, 2013, 112, 37-43.
31 M. D. Scanlon, S. K. Urszula, B. Serguei, M. A. Domhnall, L. Dónal, D. Yi and M. Edmond, *Langmuir*, 2012, **28**, 2251-2261.
32 Y. Ding, Y. J. Kim and J. Erlebacher, *Adv. Mater.*, 2004, **16**, 1897-1900.
33 W. Qin, Y. F. Zhao, C. X. Xu, W. Dan, Y. Y. Cai, H. Jing, L. He, B. Du and M. H. Yang, *Biosens. Bioelectron.*, 2011, **26**, 3714-3718.
34 Y. B. Mollamahale, M. Ghorbani, M. Ghalkhani, M. Vossoughi and A. Dolati, *Electrochim. Acta*, 2013, **106**, 288-292.
35 W. W. Tu, X. L. Fang, J. Lou and Z. H. Dai, *Analyst*, 2015, **140**, 2603-2607.
36 M. R. Mahmoudian, W. J. Basirun, P. M. Woi, M. Sookhakian, R. Yousefi, H. Ghadimi and Y. Alias, *Sci. Mater. Eng. C, Mater. Biol. Appl.*, 2016, 59, 500-508.
37 B. Rezaei, O. Rahmanian and A.A. Ensafi, *Sens. Actuators, B.* 2014, **196**, 539-545.
38 M. B. Gholivand and L. Mohammadi-Behzad, *Mater. Sci. Eng. C, Mater. Biol. Appl.*, 2015, **57**, 77-87.
39 M. B. Gholivand and L. Mohammadi-Behzad, *Mater. Sci. Eng. C, Mater. Biol. Appl.*, 2015, **48**, 235-24.
40 M. M. Ghoneim and A. Tawfik, *Anal. Chim. Acta*, 2004, **511**, 63-69.
41 L. Q. Lin, Y. C. Li, Q. Fu, L. C. He, J. Zhang, and Q. Q. Zhang, *Polymer*, 2006, **47**, 3792-3798.
42 Y. Ge and P. F. Anthony, *Chem. Eur. J.*, 2009, **15**, 8100-8107.

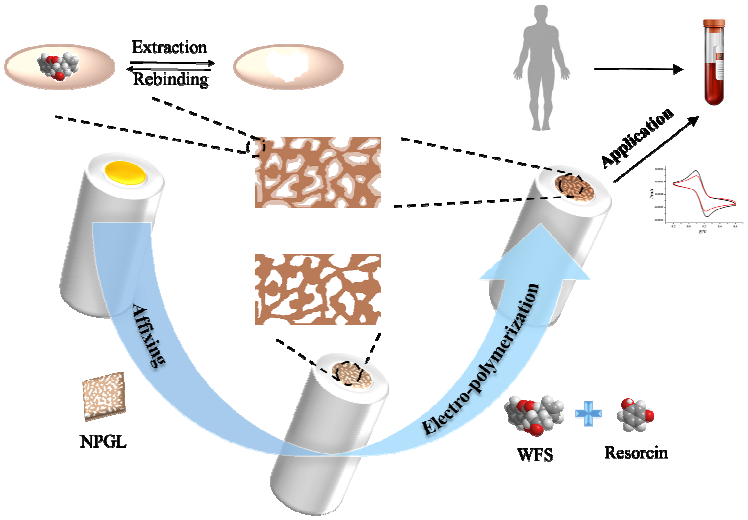


A novel electrochemical sensor was facilely fabricated by coupling nanoporous gold leaf (NPGL) with molecularly imprinted polymer (MIP) and afforded ultrasensitive and selective determination of warfarin sodium (WFS).